

Evaluation of Soil–Pipe Interaction under Relative Axial Ground Movement

Masood Meidani¹; Mohamed A. Meguid, Ph.D., P.Eng., M.ASCE²;
and Luc E. Chouinard, Ph.D., P.Eng.³

Abstract: The expansion of urban communities around the world resulted in the installation of utility pipes near existing natural or artificial slopes. These pipes can experience significant increase in axial earth pressure as a result of possible slope movement in the pipeline direction. This research aims at utilizing the discrete-element method to investigate the response of a buried pipeline in granular material subjected to axial soil movement. To determine the input parameters needed for the discrete-element analysis, calibration is performed using triaxial and direct shear test data and the microscopic parameters are determined by matching the numerical and experimental results. The soil–pipe system is then modeled and the detailed behavior of the pipe and the surrounding soil as well as their interaction at the particle-scale level are presented. Conclusions are made regarding the suitability of the empirical approach used in practice to estimate the axial soil resistance in different soil conditions. This study suggests that caution should be exercised in calculating axial soil resistance to relative pipe movement in dense sand material. A suitable lateral earth pressure coefficient should be determined in these cases as a function of the soil and pipe properties. DOI: 10.1061/(ASCE)PS.1949-1204.0000269. © 2017 American Society of Civil Engineers.

Author keywords: Soil–structure interaction; Discrete-element method (DEM); Buried pipes; Axial movement.

Introduction

Buried pipes are considered to be among the most economical and safe methods of transporting natural resources (e.g., oil, natural gas, and water distribution networks). Permanent ground deformation resulting from earthquakes or movement of nearby slopes can impose additional loads on the pipe leading to unacceptable deformation and pipe separation from the surrounding soil. A report of the European Gas Pipeline Incident Data Group (2005) has indicated that ground movement represents the fourth major cause of gas pipeline failure with close to half of the reported cases resulting in pipe rupture.

The response of buried pipes to slope movements depends on the orientation of the pipeline with respect to the moving slope. If the pipe axis is parallel to the direction of the sliding soil, the pipe would be subjected to longitudinal (axial) strains and the pipe experiences either tensile or compressive stresses. The second condition occurs when the axis of the pipe is normal to the soil movement direction and, in this case, the relative soil movement imposes lateral deformation to the pipe resulting in strains and stresses on the pipe wall due to the development of bending moments and shear forces. ASCE (1984) recommended a closed-form solution to

determine the axial loads on buried pipes in cohesionless soils using the following expression:

$$F_A = \gamma' \times H \times (\pi DL) \times \left(\frac{1 + K_0}{2} \right) \times \tan(\delta) \quad (1)$$

where F_A = axial soil resistance; γ' = soil effective unit weight; H = depth from ground surface to the pipe springline; D = pipe outer diameter; L = pipe length; K_0 = coefficient of lateral earth pressure at rest; and δ = friction angle between the soil and the pipe.

Over the past few decades, researchers have studied soil–pipe interaction using experimental, theoretical, and numerical methods (e.g., Newmark and Hall 1975; Trautmann and O'Rourke 1983; O'Rourke and Nordberg 1992; Honegger and Nyman 2002; Chan and Wong 2004; Karimian et al. 2006; Wijewickreme et al. 2009; Daiyan et al. 2011; Rahman and Taniyama 2015; Liu et al. 2015; Almahakeri et al. 2016; Zhang et al. 2016). Most of the numerical analyses were performed using the finite-element (FE) method. Yimsiri et al. (2004) used FE analysis to study soil–pipe interaction under lateral and upward soil movements in a deep burial condition. Guo and Stolle (2005) investigated the lateral earth pressure on buried pipes and concluded that capturing large soil movement interacting with a buried conduit is challenging using continuum approaches. Almahakeri et al. (2016) conducted a series of three-dimensional (3D) FE simulations to examine the longitudinal bending in buried glass fiber–reinforced polymer (GFRP) pipes subjected to lateral earth movements and compared the results with measured data. Most recently, Zhang et al. (2016) studied the mechanical behavior of a buried steel pipeline crossing a landslide area using finite-element analysis and highlighted the role of soil and pipeline parameters on the behavior of the system. Although soil–structure interaction with large deformation can be modeled using a multiscale approach (Hughes 1995) or adaptive remeshing (Zienkiewicz and Huang 1990), modeling particle movement and unpredictable discontinuities near existing pipes is very scarce in the literature.

The discrete-element method (DEM) has proven to be suitable for modeling granular material and large deformation. The method

¹Graduate Student, Dept. of Civil Engineering and Applied Mechanics, Univ. of McGill, 817 Sherbrooke St. W., Montreal, QC, Canada H3A 0C3. E-mail: masood.meidani@mail.mcgill.ca

²Associate Professor, Dept. of Civil Engineering and Applied Mechanics, Univ. of McGill, 817 Sherbrooke St. W., Montreal, QC, Canada H2A 0C3 (corresponding author). ORCID: <http://orcid.org/0000-0002-5559-194X>. E-mail: mohamed.meguid@mcgill.ca

³Associate Professor, Dept. of Civil Engineering and Applied Mechanics, Univ. of McGill, 817 Sherbrooke St. W., Montreal, QC, Canada H2A 0C3. E-mail: luc.chouinard@mcgill.ca

Note. This manuscript was submitted on September 14, 2016; approved on January 6, 2017; published online on March 25, 2017. Discussion period open until August 25, 2017; separate discussions must be submitted for individual papers. This paper is part of the *Journal of Pipeline Systems Engineering and Practice*, © ASCE, ISSN 1949-1190.

was first proposed by Cundall and Strack (1979) and has been used to analyze various geotechnical engineering problems. Laboratory tests have been successfully modeled by researchers using DEM to investigate the microscopic behavior of soil samples. Cui and O'Sullivan (2006) used discrete elements to study the macroscopic and microscopic behavior of granular soil under direct shear test conditions. Tran et al. (2013) proposed a finite-discrete element framework for the 3D modeling of geogrid-soil interaction under pullout loading condition. Also, Tran et al. (2014) conducted three-dimensional discrete-element analysis to study the earth pressure distribution on cylindrical shafts. The analysis allowed for the soil arching and radial pressure on the shaft wall to be visualized. Furthermore, Ahmed et al. (2015) conducted laboratory experiments and finite-discrete element analysis to study the role of geogrid reinforcement in reducing earth pressure on buried pipes. It has been shown in these studies that discrete-element or coupled finite-discrete element approaches are effective in capturing the response of structural elements such as pipe and geogrid and their interaction with the surrounding soils.

This study presents the results of a three-dimensional discrete-element investigation that has been conducted to examine the response of a steel pipe buried in dense granular material and subject to axial loading. A suitable discrete-element packing method is first utilized to prepare a soil sample with predefined properties. Material calibration is then performed using standard triaxial and direct shear tests to determine the input parameters needed for the discrete-element simulation. The calculated response of the pipe is compared with the reported experimental results. The validated model is used to determine the distribution of radial earth pressure on the pipe wall and understand the changes in in situ pressure around the pipe during and after the pullout process. The applicability of the available closed-form solution is also evaluated.

Discrete-Element Method

The DEM generally models the interaction between particles as a dynamic process that reaches static equilibrium when the internal and external forces are balanced. Displacement and rotation of each particle are usually determined using Newton's and Euler's equations. The discrete-element simulations reported in this study are performed using the open source code *YADE* (Kozicki and Donzé 2008; Šmilauer et al. 2010). Spherical particles of different sizes are adopted to represent the grain size distribution of the backfill soil. The contact law between particles is selected from the *YADE* library. It includes Cundall's linear elastic-plastic law with capability of transmitting moments between particles. The contact law is briefly described as follows:

Following the collision of two particles A and B with radii r_A and r_B , contact penetration depth is defined as

$$\Delta = r_A + r_B - d_0 \quad (2)$$

where d_0 = distance between the centers of particles A and B.

Particle interaction is represented by the force vector \mathbf{F} . This vector can be decomposed into normal and tangential forces

$$F_N = K_N \cdot \Delta_N, \delta F_T = -K_T \cdot \delta \Delta_T \quad (3)$$

where F_N = normal force; δF_T = incremental tangential force; K_N and K_T = normal and tangential stiffnesses at the contact point; Δ_N = normal penetration between the particles; and $\delta \Delta_T$ = incremental tangential displacement between the two particles.

The normal stiffness between particles A and B at the contact point is defined by

$$K_N = \frac{K_N^A \cdot K_N^B}{K_N^A + K_N^B} \quad (4)$$

where K_N^A and K_N^B = particle normal stiffnesses calculated using particle radius r and material modulus E as follows:

$$K_N^A = 2E_A r_A \quad \text{and} \quad K_N^B = 2E_B r_B \quad (5)$$

Therefore, the normal stiffness at the contact point can be written as

$$K_N = \frac{2E_A r_A \cdot 2E_B r_B}{2E_A r_A + 2E_B r_B} \quad (6)$$

The interaction tangential stiffness K_T is defined as a ratio of the computed K_N such that $K_T = \alpha K_N$.

The tangential force is limited by a threshold value expressed as

$$F_T = \frac{F_T}{\|F_T\|} \|F_N\| \cdot \tan(\phi_{\text{micro}}) \quad \text{if } F_T \geq \|F_N\| \cdot \tan(\phi_{\text{micro}}) \quad (7)$$

where ϕ_{micro} = microscopic friction angle between particles.

The rolling resistance is determined using a rolling angular vector $\boldsymbol{\theta}_r$ obtained by summing the components of the incremental rolling (Šmilauer et al. 2010)

$$\boldsymbol{\theta}_r = \sum d\boldsymbol{\theta}_r \quad (8)$$

A resistant moment M_r is calculated by

$$M_r = K_r \cdot \boldsymbol{\theta}_r \quad (9)$$

where K_r = rolling stiffness of the interaction defined as

$$K_r = \beta_r \cdot \left(\frac{r_A + r_B}{2} \right)^2 \cdot K_T \quad (10)$$

The resistant moment is limited by a threshold value such that

$$M_r = \frac{\boldsymbol{\theta}_r}{\|\boldsymbol{\theta}_r\|} \cdot \eta_r \cdot \|F_N\| \cdot \left(\frac{r_A + r_B}{2} \right) \quad (11)$$

if $K_r \cdot \boldsymbol{\theta}_r \geq \eta_r \cdot \|F_N\| \cdot \left(\frac{r_A + r_B}{2} \right)$

where η_r = dimensionless coefficient; and β_r = rolling resistance coefficient.

To ensure the stability of the DEM model, the critical time step Δt_{cr} is defined as

$$\Delta t_{cr} = \min_i \sqrt{2} \cdot \sqrt{\frac{m_i}{K_i}} \quad (12)$$

where m_i = mass of particle i ; and K_i = per-particle stiffness of the contacts in which particle i participates and \min_i indicates the minimum value.

Description of the Numerical Model

The experimental results used to validate the numerical model are based on those reported by Wijewickreme et al. (2009). The response of a buried steel pipe subjected to axial soil movement was investigated in a test chamber (3.8 m long, 2.5 m wide, and 1.82 m high) as depicted in Fig. 1. Graded Fraser River sand with in situ density of 16 kN/m³ was used as a backfill soil. The mechanical characteristics of the sand have been also reported based on triaxial and direct shear tests conducted under confining

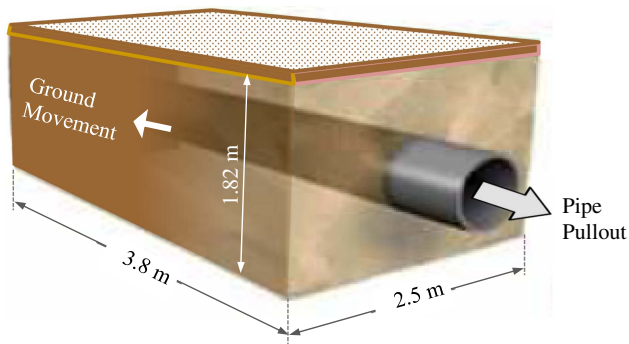


Fig. 1. Configuration of the modeled experiments

Table 1. Mechanical Characteristics of Fraser River Sand

| Parameter | Value |
|--|-------|
| Particle density (kg/m^3) | 2,720 |
| ϕ_{peak} (degrees) | 45 |
| ϕ_{cv} (degrees) | 33 |
| ψ (degrees) | 15 |
| Cohesion (kN/m^2) | 0 |
| E_i (MPa) | 36 |
| ν | 0.3 |
| γ (kg/m^3) for $D_r = 75\%$ (dense sand) | 1,600 |

pressures that range from 15 to 50 kPa. A summary of the mechanical characteristics of the backfill soil is given in Table 1. The steel pipe used in the experiments has an outside diameter of 46 mm and a wall thickness of 13 mm. The interface friction angle (δ) between the backfill material and the steel pipe was reported to be 36° . The pipe is placed over 0.7 m of bedding layer up to the springlines and covered with 1.15 m of the backfill material. This corresponds to a height-to-diameter ratio (H/D) of 2.5.

The numerical model has been developed in this study such that it replicates the geometry and test procedure used in the experiments. All components are generated inside the YADE package. Various packing algorithms can be used to generate DEM samples for both standard soil tests and large-scale pullout simulations. Techniques such as the compression method (Cundall and Strack 1979), gravitational method (Ladd 1978), triangulation-based approach (Labra and Oñate 2009), and radius expansion method (PFC 2D) are widely used for this purpose.

Generating the Discrete-Element Particles

The soil sample is generated in this study using the radius expansion method following a grain size distribution similar to that of the backfill material. Given the size of the physical model, it is numerically impractical to simulate millions of particles with their actual size. Therefore, particle upscaling with two different scale factors has been adopted to gradually reduce the number of particles and maintain the time step size at a reasonable value. In this process, a balance between the computational costs and the scaling effects on the global response needs to be considered. The soil in the test chamber is divided into four zones as illustrated in Fig. 2. A particle scale factor of 90 is used in Zone 1, which represents the area immediately around the pipe, and increases to 140 in the remaining zones. A small scale factor is applied to particles in the close vicinity of the pipe to improve the contact between the soils and pipe. The selected scale factors are also supported by the findings of

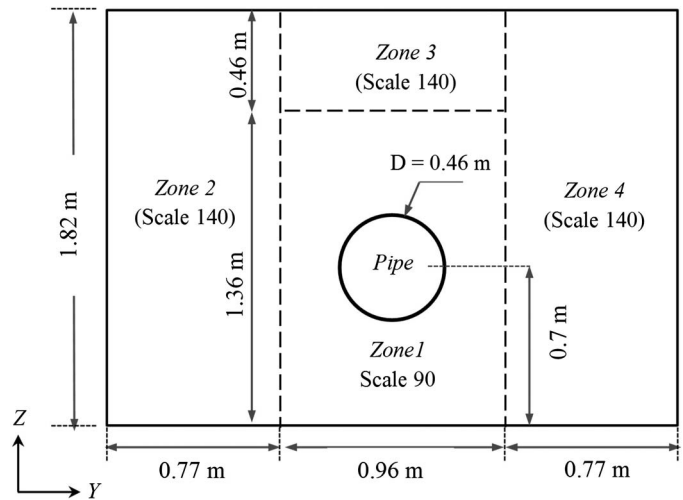


Fig. 2. Schematic showing the different particle packing zones around the pipe

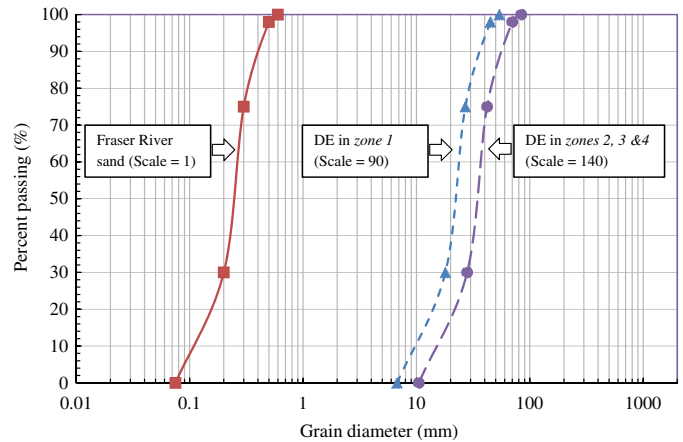


Fig. 3. Grain size distribution with particle upscaling

previous researchers. Potyondy and Cundall (2004) noted that when the number of particles used in a discrete-element simulation is large enough (more than 265,000 particles in this study using the mentioned scale factors), the macroscopic response becomes independent of the particle size. Also, Tran et al. (2014) evaluated the effect of different scale factors in analyzing soil–structure interaction and confirmed that when the number of particles is greater than 245,000, the scale factor has an insignificant effect on the overall response of the system. Furthermore, Ahmed et al. (2015) suggested that creating a DEM sample with the number of soil particles around 300,000 makes the global response of the system insensitive to the change in particle size. The grain size distributions of the backfill material and the particles in the different zones are shown in Fig. 3.

A cloud of noncontacting particles is first generated inside the box for each zone following a predetermined particle size distribution and scale factor. Particles located within the pipeline area are then removed. The radius expansion method is applied to each zone to achieve a target porosity of 0.41, which corresponds to that of the experiment. The radius expansion method is known to generate a specimen with an isotropic stress state (O’Sullivan 2011). To dissipate this effect, each zone was subjected to gravity forces and allowed to reach equilibrium. The entire packing, including the four different zones, is then assembled under gravity

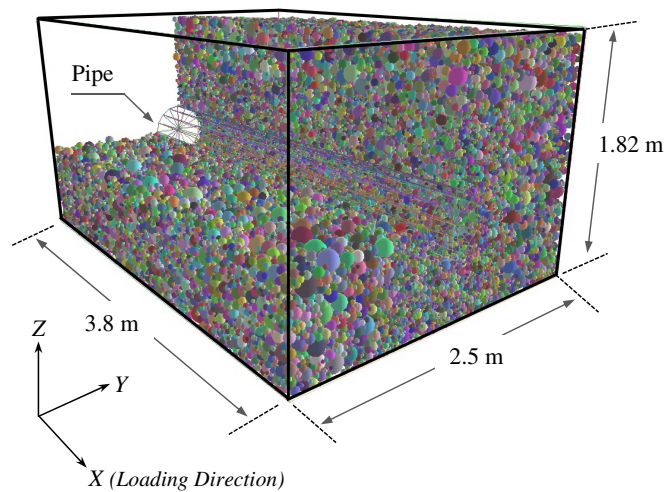


Fig. 4. Partial view of the model showing the pipe and surrounding soil

and the homogeneous distribution of the contact forces is checked using the fabric tensor. The total number of particles used in the final packing is approximately 265,000. It has been found that the fabric tensor components are nearly identical with θ_{xx} and θ_{yy} of approximately 0.33 and θ_{zz} of approximately 0.34, where z is the gravitational direction. A partial view of the packing including the pipeline and its surrounding spherical particles is shown in Fig. 4. To further illustrate the distribution of particle sizes in the vicinity of the pipe, a close view of the pipe and the nearby zones is also provided in Fig. 5(a).

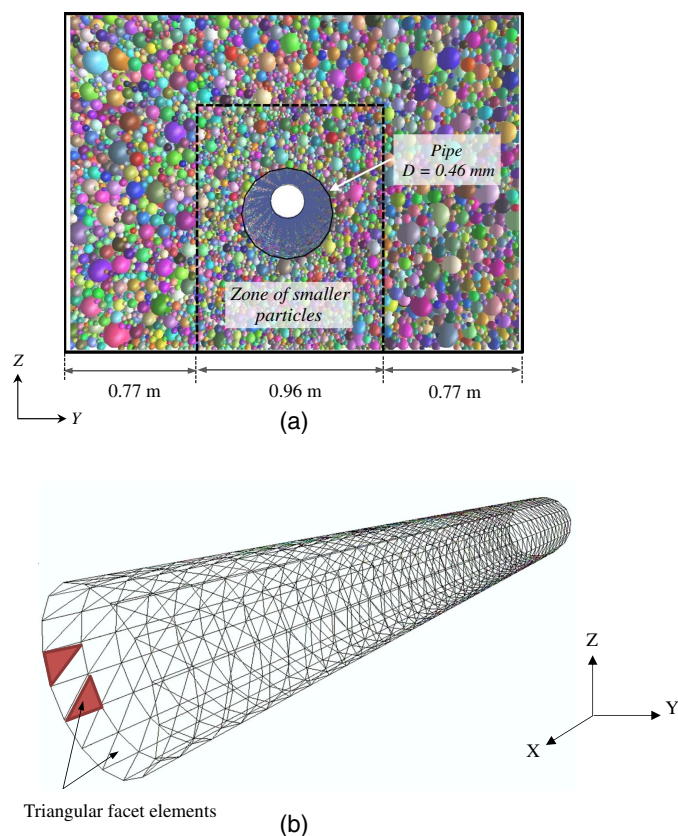


Fig. 5. Numerical model: (a) particle distribution in the close vicinity of the pipe; (b) simulated pipeline using facet elements

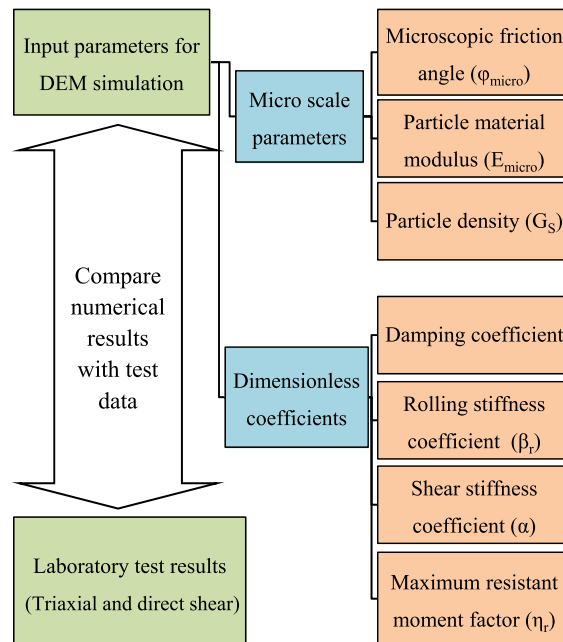


Fig. 6. Input parameters required for the material calibration and the large-scale discrete-element analysis

The pipe is modeled in this study using triangular facet elements (flat discrete elements) with material modulus comparable to that of the steel pipe. The interface friction angle between the facet elements and the soil particles is known to play an important role in the analysis and needs to be properly chosen, as explained in the next sections. The pipe wall is modeled using a total of 1,216 facet elements arranged in a hexadecagonal shape. The length of the pipe is chosen such that it extends slightly outside the back of the chamber to ensure continuous contact with the soil during the pullout process. A 3D view of the simulated pipe is presented in Fig. 5(b).

Material Calibration

Input parameters used in the discrete-element simulation include two major groups: (1) physical parameters (friction angle, cohesion, and Young's modulus), and (2) dimensionless coefficients (e.g., rolling and shear stiffness coefficients, maximum resistant moment factor). A calibration procedure is required to determine these input parameters for a given soil condition before it is adopted in the DEM. The model used in this study is calibrated by simulating triaxial tests conducted on Fraser River sand (Karimian 2006) and comparing the calculated response with the measured values. In addition, direct shear tests are also modeled to confirm the input parameters to be used in the pullout simulation. A flowchart that summarizes the calibration process and the different microparameters needed for the DEM simulation is given in Fig. 6.

Triaxial Test

The numerically simulated triaxial test [Fig. 7(a)] consists of a rectangular prism with an aspect ratio of 2 (76 mm long, 76 mm wide, and 152 mm high) to approximate the geometry of the tested samples. The particle assembly is created using the radius expansion method described in the previous section. The final pack contains more than 23,000 spherical particles with a porosity of 0.41 (dense sand) and grain size distribution similar to that of the real sand

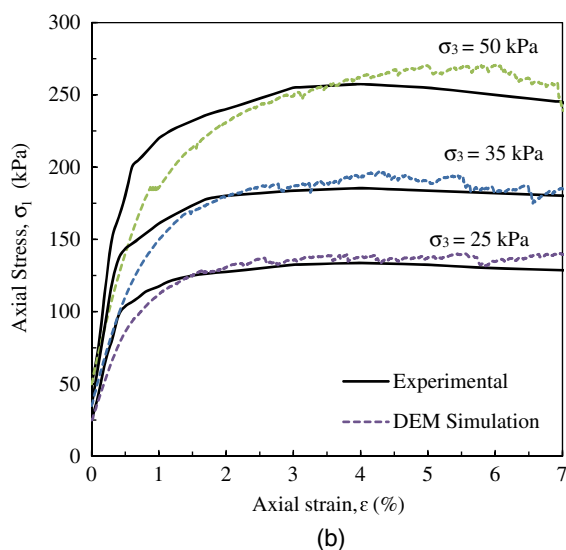
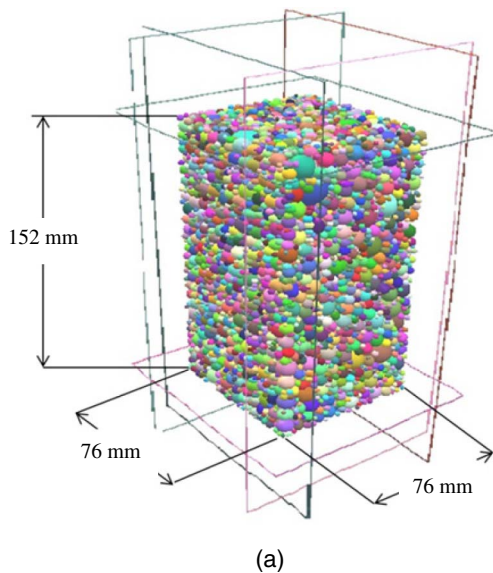


Fig. 7. Triaxial tests used for the material calibration: (a) tested sample; (b) results

material. The numerical simulation includes two stages: (1) the sample is compressed up to a target confining stress of 25, 35, or 50 kPa; and (2) the top wall is allowed to move downward at a constant strain rate to impose the deviatoric load while the stresses at the side walls are kept constant.

The interaction between particles is simulated using a contact model that considers traction, compression, bending, and twisting with cohesion and friction based on Mohr-Coulomb failure criterion. Plassiard et al. (2009) proposed a calibration procedure that involves elastic parameters (E , K_T/K_N , β_r) as well as rupture parameters (ϕ_{micro} and η_r). These parameters are determined to satisfy the correct shape of the stress-strain curve and match the initial Young's modulus E_i , Poisson's ratio ν , dilation angle ψ , and friction angle ϕ of the material. The calibration is performed for a confining pressure of 25 kPa and the obtained parameters are confirmed by repeating the analysis for confining pressures of 35 and 50 kPa. Fig. 7(b) presents the results of the discrete-element analysis along with the experimental data for all ranges of confining pressures. The soil properties obtained from the triaxial test simulation for confining pressure of 25 kPa are summarized in Table 2.

Table 2. Soil Properties Based on Triaxial Tests with 25-kPa Confining Stress

| Parameter | Value |
|--------------------------------|-------|
| ϕ_{peak} (degrees) | 45 |
| ψ (degrees) | 15 |
| E_i (MPa) | 34 |
| ν | 0.28 |

Table 3. Selected Properties Used in Discrete-Element Analysis

| Parameter | Value |
|---|-------|
| Particle density (kg/m^3) | 2,720 |
| Particle material modulus E (MPa) | 150 |
| K_T/K_N ratio | 0.7 |
| β_r | 0.15 |
| ϕ_{micro} (degrees) | 35 |
| η_r | 1 |
| Damping ratio | 0.2 |

Direct Shear Test

Modeling the direct shear test is used to confirm the macroscopic and microscopic parameters (Tables 2 and 3) to be used in the simulation. The direct shear test ($60 \times 60 \times 25$ mm) was based on that reported by Karimian (2006) for Fraser River sand under three different normal stresses (20, 35, and 53 kPa). The discrete-element packing used in the direct shear test was created such that it has similar characteristics as that described in the triaxial test including porosity, coordination number (N_c), and fabric tensor (Φ_{ij}). The sample porosity and coordination numbers at the initial state were found to be 0.41 and 5.5, respectively. As shown in Fig. 8(a), a specimen is created using the radius expansion method with a total of 24,688 spheres and using a scale factor 5. The input parameters given in Table 3 are then assigned to the particles. The results of the direct shear test for different normal stresses is shown in Fig. 8(b). The overall trend and the maximum shear stress values are found to be consistent with the laboratory results. A slightly softer response is observed for shear displacements of less than 0.5 mm. This may be attributed to the difference in particle shapes as compared to the spherical particles used in the discrete-element analysis. Similar observation was made by Yan (2008).

Modeling the Pullout Procedure

Following the material calibration, a final specimen is created and the properties are assigned to the discrete particles. No friction is used for the interaction between the particles and the walls of the box, which is similar to the condition of the experiments to eliminate the boundary effects. A parametric study is conducted to examine the effect of friction angle of the facets (used to model the pipe) on the pullout response. Results indicated that the soil-pipe system is sensitive to the interface friction and a friction angle of 30° was found to correspond to a maximum pullout force that matches the experimental data.

The pullout procedure is numerically simulated under displacement control with a movement rate of 50 mm/s applied to the facets to be consistent with the experiment. The pipe was incrementally pulled until a maximum displacement of 200 mm was reached. The corresponding pullout force is captured during the simulation by summing the forces on the facets in the pulling direction.

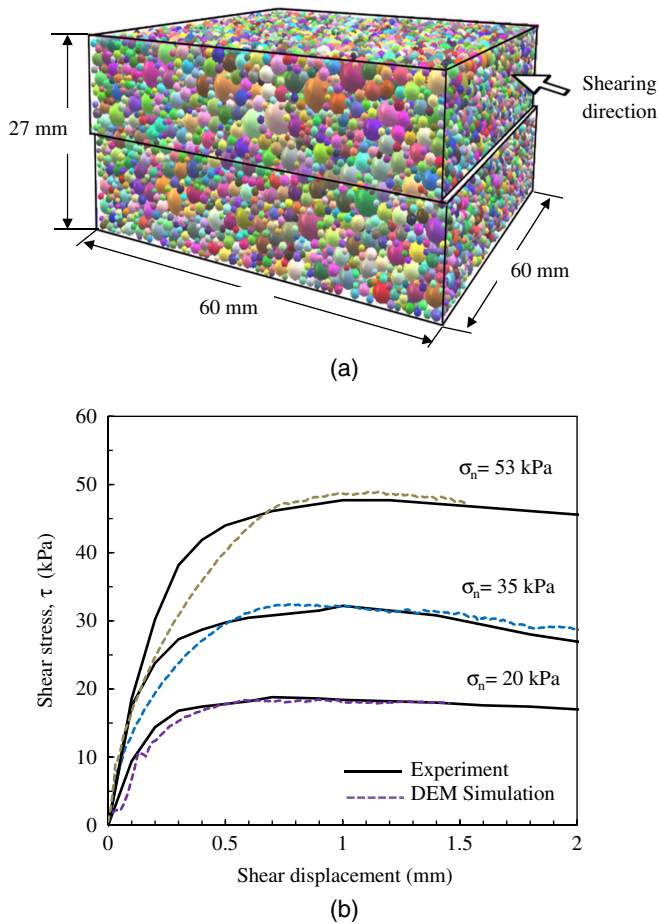


Fig. 8. Direct shear tests used to confirm the input parameters: (a) tested sample; (b) results

Radial Earth Pressure Distribution

After the final particle assembly in the chamber and the assignment of input parameters, the pipe and the surrounding particles were allowed to freely move under gravity. The initial stress distribution acting on the pipe is examined and compared with the analytical solution. The equation proposed by Hoeg (1968) allows for the radial pressure (σ_r) on buried pipes to be determined as follows:

$$\sigma_r = \frac{1}{2} P \left\{ (1+k) \left[1 - a_1 \left(\frac{D}{2r} \right)^2 \right] - (1-k) \left[1 - 3a_2 \left(\frac{D}{2r} \right)^4 - 4a_3 \left(\frac{D}{2r} \right)^2 \right] \cos 2\theta \right\} \quad (13)$$

where D = pipe diameter; r = distance from the pipe center to the soil element under analysis; k = lateral earth pressure coefficient at rest; P = soil vertical stress; θ = angle of inclination from the spring-line; and a_1 , a_2 , and a_3 = constants.

A comparison of the initial radial pressures calculated using DEM and that of Hoeg's solution at selected locations is shown in Fig. 9. The pressure values are presented on opposite sides of the polar chart. The contact pressure ranged from 15 kPa at the crown (angle 0°) to approximately 20 kPa at the invert (angle 180°), which is consistent with the expected distribution for rigid pipes.

Vertical stress distribution in soil is also examined and compared with the expected values. To record macroscopic stress

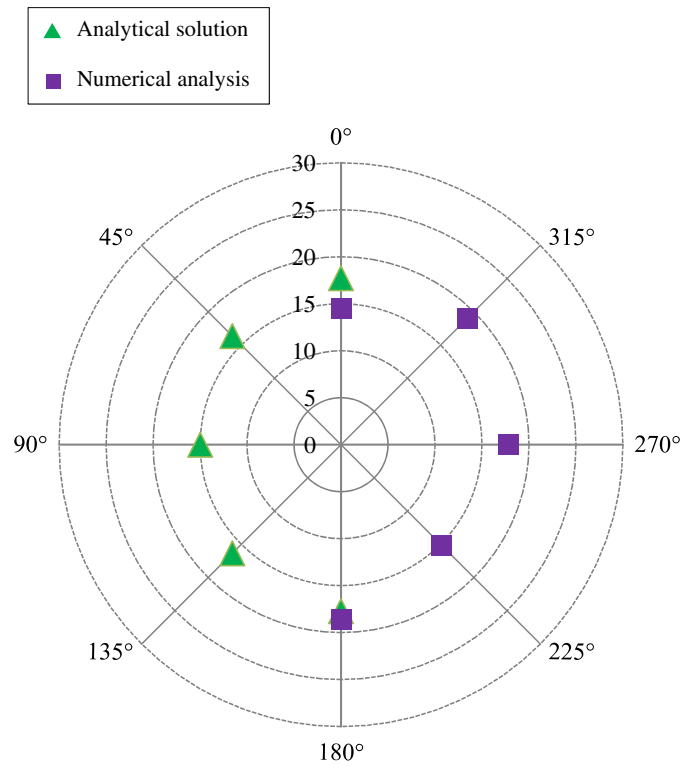


Fig. 9. Initial earth pressure distribution on the pipe (kPa)

components, a measurement box of volume V is used and the average stress within the box is calculated as

$$\sigma_{ij} = \frac{1}{V} \sum_{c=1}^{N_c} \mathbf{x}^{c,i} \mathbf{f}^{c,j} \quad (14)$$

where N_c = number of contacts within the measurement box; $\mathbf{f}^{c,j}$ = contact force vector at contact c ; $\mathbf{x}^{c,i}$ = branch vector connecting two contact particles A and B; and indexes i and j are the Cartesian coordinates.

The soil chamber is divided into three regions [Fig. 10(a)] and the vertical stresses are calculated in each region using Eq. (14). Region 1 is selected near the wall to evaluate the effect of the rigid boundaries on the results. Regions 2 and 3 are chosen at the same distance in the opposite side of the pipe to assess the homogeneity of the generated particle packing. Vertical stresses are obtained using measurement boxes with dimensions of $0.25 \times 0.25 \times 0.25$ m and the results are presented in Fig. 10(b). It can be seen that vertical stress distribution in Region 1 near the boundary is consistent with the expected values ($\gamma'z$). This signifies that the effect of the walls on the calculated vertical soil pressures is negligible. In addition, by comparing the vertical stress distribution in Regions 2 and 3, it is evident that the particle packing used in the simulation is homogenous.

Evaluating the Applicability of the Closed-Form Solution

The relationship between the pullout force and corresponding pipe displacement is shown in Fig. 11. To facilitate comparison between the numerical and experimental results, the axial resistance F_A is normalized with respect to soil density (γ'), pipe length (L), depth (H), and diameter (D) as represented by Eq. (15)

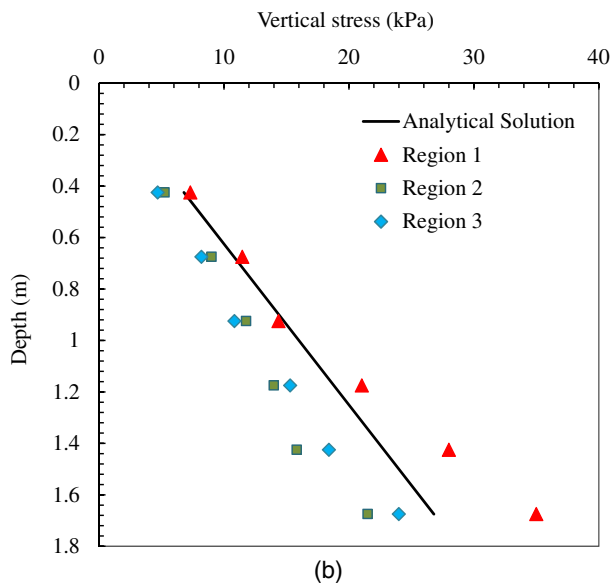
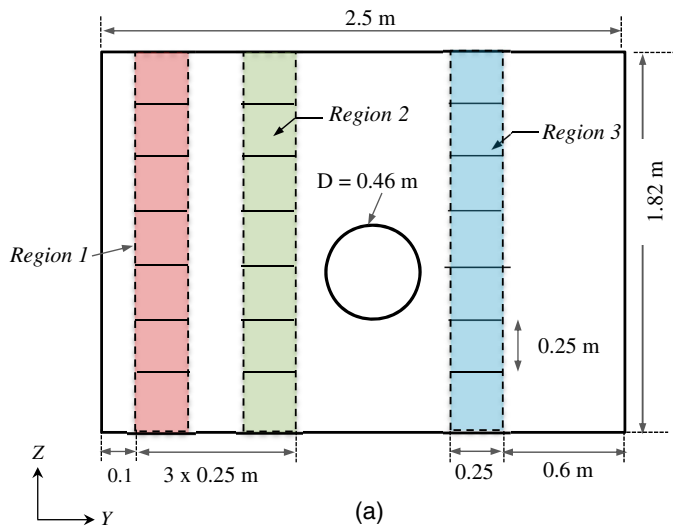


Fig. 10. Comparing in situ stresses with analytical solution: (a) selected soil; (b) vertical stress distributions

$$F'_A = \frac{F_A}{\gamma' \times H \times \pi \times D \times L} \quad (15)$$

The calculated pullout response (Fig. 11) shows a peak normalized axial force F'_A of approximately 1.0 at pipe displacement of approximately 9–12 mm with postpeak value of 0.89 after reaching axial displacement of approximately 115 mm. The overall response of the soil–pipe system is found to be reasonably captured by the model and the calculated peak value of the pullout force is similar to the measured value with 20% overestimation in postpeak resistance. Because the maximum axial soil resistance (pullout force) is of prime importance in this case, and given the simplified nature of the DEM model, the calculated response is considered to be acceptable.

The normalized pullout load (F'_A) is compared with the maximum axial load recommended by ASCE (1984). Eq. (1) is used to determine the peak pullout load, F_A , where the K_0 value ($K_0 = 1 - \sin \phi'$) is calculated using ϕ' of 44° and the interface friction angle (δ) is assumed to be 36° . This corresponds to the reported peak friction angle of Fraser River sand. Fig. 12 shows the

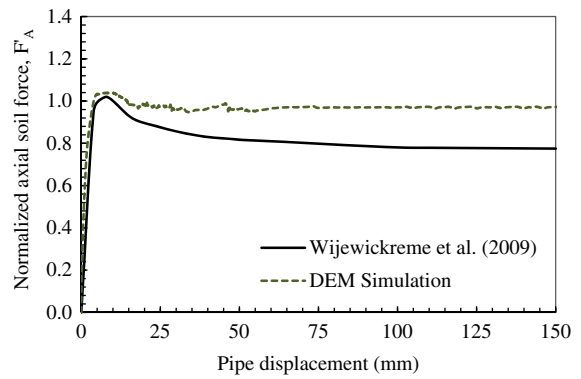


Fig. 11. Comparison between calculated and measured pullout response of the pipe

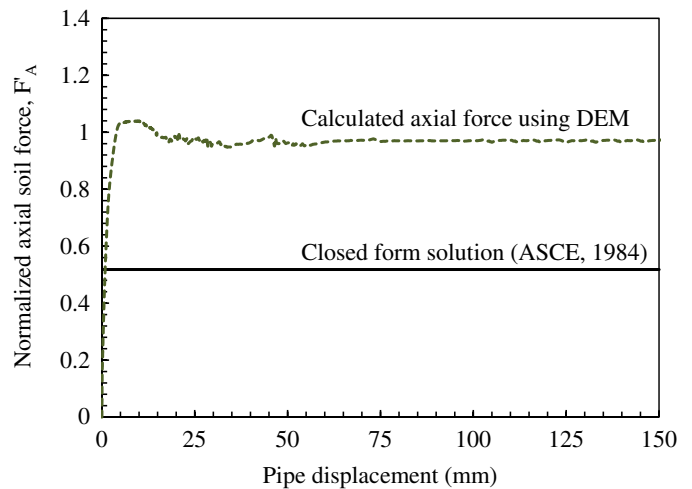


Fig. 12. Normalized soil load (F'_A) in the axial direction versus pipe displacement

normalized axial pullout load (F'_A) obtained using DEM and peak axial soil resistance calculated based on the ASCE recommendation. It can be seen that for the material investigated in this study, the ASCE formula resulted in a significantly lower peak pullout load as compared to that calculated using DEM. Among the parameters in Eq. (1), the use of the K_0 value under these loading conditions seems to be unrealistic. The discrepancy between the analytical and numerical solutions arises mainly from the underestimated normal stresses. To investigate the role of normal stresses on the pullout load, the calculated pressure acting on the pipe before (at rest) and during the pullout test (at peak pullout load) are plotted in Fig. 13. For comparison purposes, the distributions of pressure on the pipe before and after pullout are presented on opposite sides of the polar chart. It is clear that normal stresses on the pipe during the pullout are higher as compared to the at-rest condition. It is, therefore, possible to back-calculate the value of K using the average normal stresses acting on the pipe. For the given soil density (dense sand) and pipe depth (γ' of 16 kN/m^3 and H of 1.12 m), the average normal stress on the pipe at the end of the pullout procedure is found to be approximately 23 kN and the corresponding K value is approximately 1.6.

Fig. 14 presents the normalized maximum axial force (F'_A) for different values of K calculated at a constant friction angle between

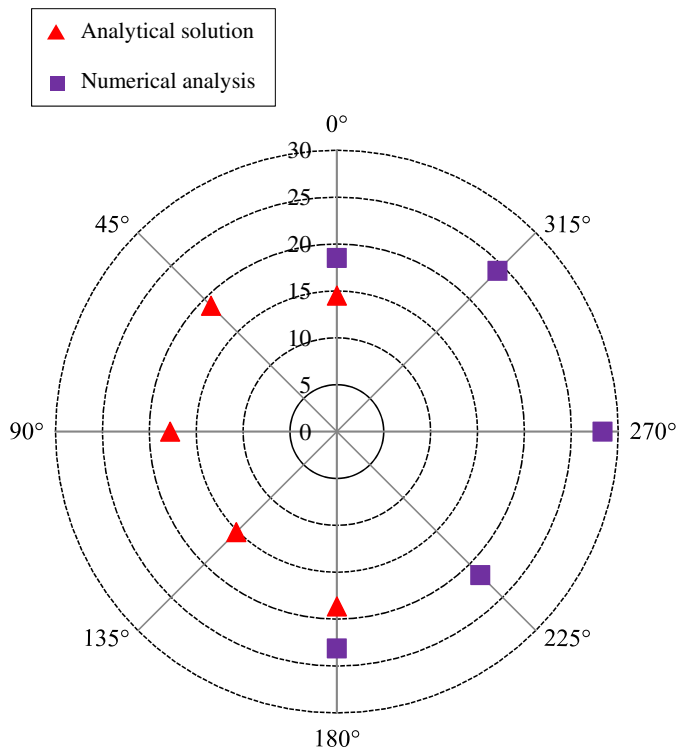


Fig. 13. Normal stress distribution on the pipe before and after the pullout test (kPa)

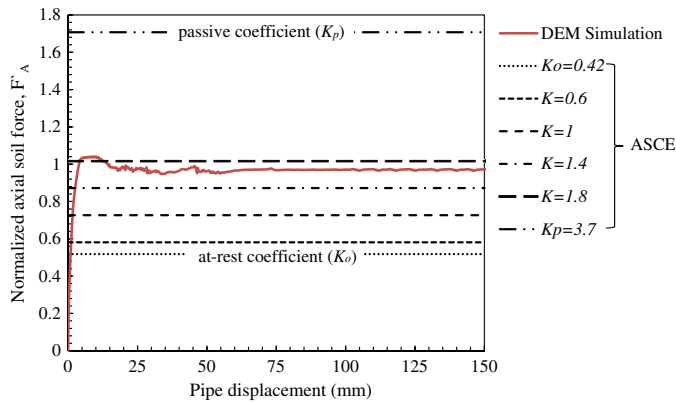


Fig. 14. Normalized axial soil resistance using ASCE (1984) equation for different K values

the pipe and the backfill material ($\delta = 36^\circ$). A lateral earth pressure coefficient K of 1.8 was found to correspond to a reasonable agreement between the maximum axial soil resistance from the DEM results and that calculated using Eq. (1). The back-calculated value of K based on the average normal stress on the pipe during pullout is found to be equal to 1.6.

It is evident from Fig. 14 that using K_o to represent the earth pressure on the pipe under pullout loading condition is not suitable, particularly for dense sand. The suggested value by ASCE (1984) for predicting the maximum axial soil resistance may be more suitable for loose to medium backfill material. This can be attributed to the dilation of dense sand that develops in the close vicinity of the pipe under large displacement resulting in a stress state that exceeds the at-rest condition.

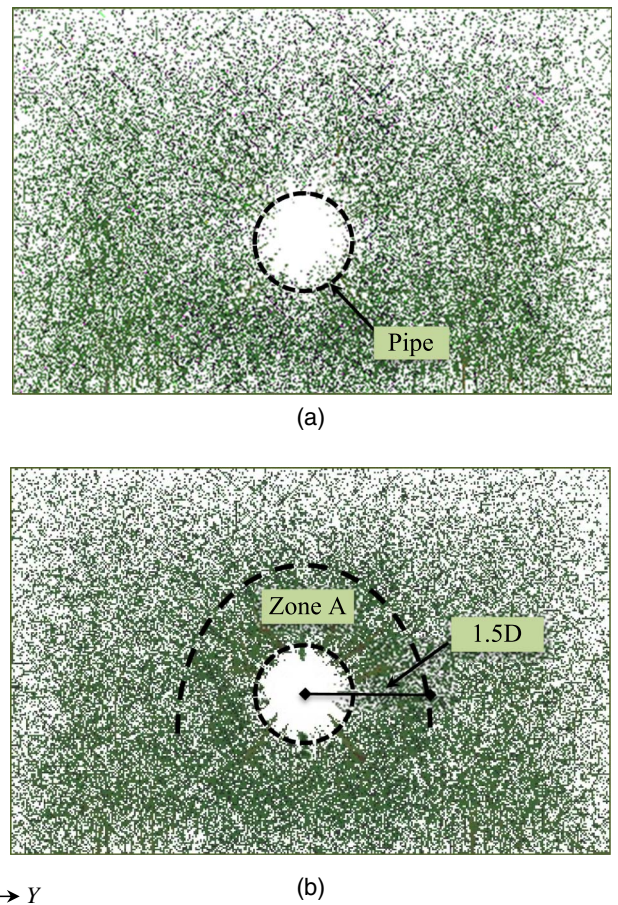


Fig. 15. Contact force network: (a) before pullout; (b) after pullout

Soil Response to Pipe Movement

To illustrate the changes that develop in the backfill material around the pipe as a result of the relative movement, the contact force network before and after the pullout test in both the transverse and longitudinal directions are shown in Figs. 15 and 16, respectively. Each contact force is illustrated by a line connecting the centers of two contacting elements, while the width of the line is proportional to the magnitude of the normal contact force. Fig. 15(a) shows that the density of the contact forces is homogeneous around the pipe before applying the pullout load. As the pipe is pulled [Fig. 15(b)], soil particles start to move, resulting in volume change and an increase in normal stresses acting on the pipe. This behavior is manifested in the large contact forces observed in the vicinity of the pipe.

The pullout effect can be further examined by inspecting the contact force distribution within the soil zones that are most affected by the pullout process. Zone A in Fig. 15(b) represents the extent of the disturbed area around the pipe selected by comparing the density of the contact forces around the pipe before and after the pullout process. The shape of this zone resembles a circle with radius of approximately 1.5 times the pipe diameter ($1.5D$). Contact forces are found to be denser and oriented radially within this zone.

Fig. 16 presents the variation in contact forces in the longitudinal direction looking downward at the soil surface. The results are presented for the initial condition [Fig. 16(a)] and after pullout [Fig. 16(b)]. As the pipe is pulled out, the density of contact forces increased along the pipe (Zone B) with further increase in density

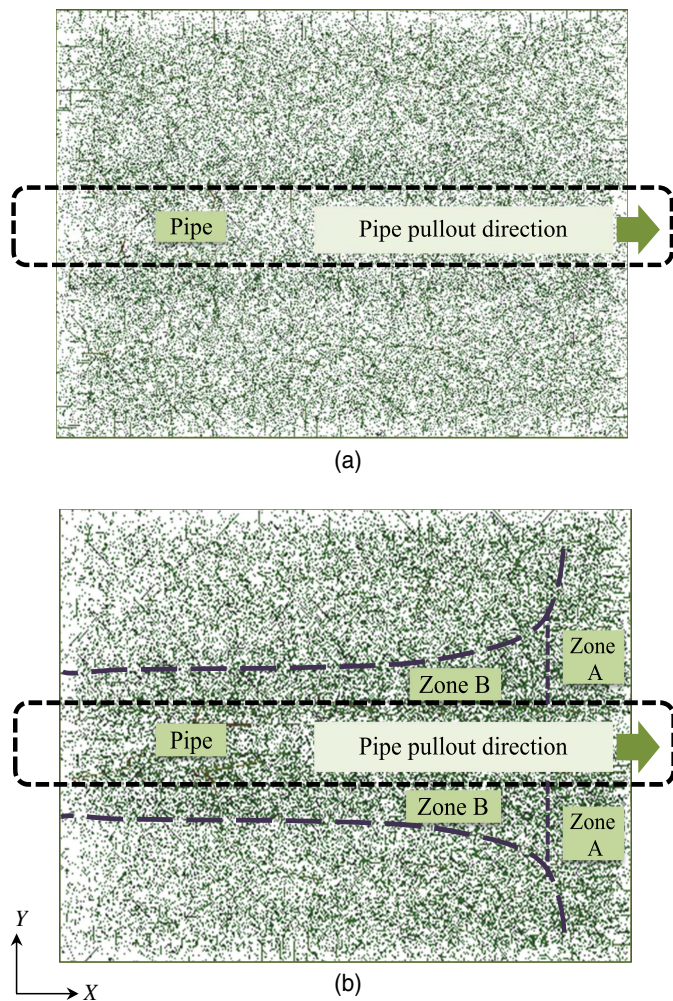


Fig. 16. Top view of the contact force network: (a) before pullout; (b) after pullout

near the front face of the box (Zone A), which is consistent with the progressive particle movement in the pullout direction.

Displacement fields across the soil domain in X (pullout) direction are shown in Fig. 17. Three different displacement fields are plotted at three elevations from the base of the chamber with $z = 1.13$ m the closest to the pipe crown. The displacement results at the three investigated sections [Figs. 17(a–c)] demonstrate that the pullout effect resulted in not only pipe movement but propagated into the surrounding soil as well. It has been found that most of the soil movement occurred in the close vicinity of the pipe and progressed incrementally in the pullout direction.

Summary and Conclusions

In this paper, a 3D numerical study was conducted to investigate the behavior of a steel pipe buried in dense sand material and subjected to axial soil movements. A discrete-element model was developed and used to simulate the pipe pullout process. Particles were generated to match the particle size distribution of the Fraser River sand and capture some of the important mechanical properties of the material. Calibration was performed to determine the input parameters needed for the discrete-element analysis using triaxial and direct shear test results. The vertical stress distribution within the soil domain as well as the initial radial pressure on the pipe were

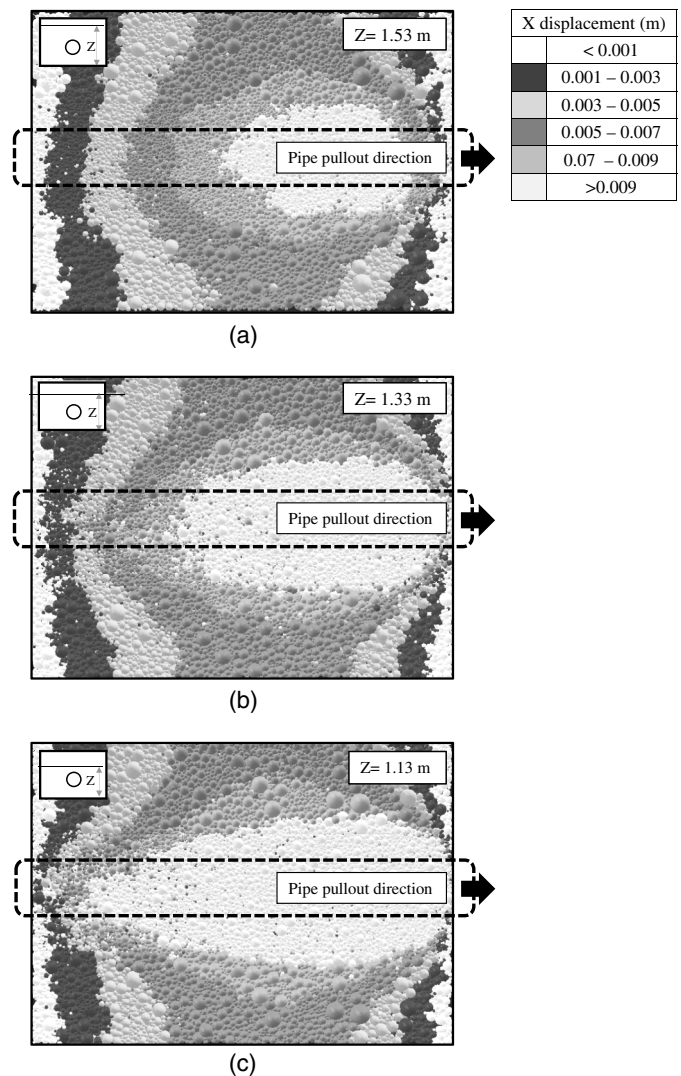


Fig. 17. Plan view showing the soil particle displacement in the horizontal direction at different elevations: (a) $Z = 1.53$ m; (b) $Z = 1.33$ m; (c) $Z = 1.13$ m

calculated. Pipe pullout was numerically simulated and the results compared with the available experimental data and closed-form solutions. The axial soil resistance and normal stress distribution on the pipe were analyzed.

The results of the discrete-element analysis of the pullout test are found to agree with the experimental data. The maximum soil resistance in the axial direction is higher than that predicted using the recommended closed-form solution reported in ASCE (1984).

The measured soil stresses acting on the pipe under the pulled loading condition in dense sand material are significantly higher compared to the initial radial stresses before the pullout. This increase in radial stresses on the pipe can be explained by the dilation of the dense sand during shear deformation. Hence, the soil condition surrounding the pipe is not considered at rest and a new lateral pressure coefficient K (as opposed to K_0) needs to be determined for the calculation of peak axial resistance of the soil. It can be concluded that the equation recommended in ASCE (1984) needs to be used with caution to calculate axial soil resistance on a buried pipe placed in a relatively dense sand material. A stifflateral earth pressure coefficient (K) should be considered as a function of the soil and pipe properties. The results of this

investigation suggest that a range of values between K_o and 2 is considered to be reasonable for pipelines under similar conditions. The numerical modeling approach proposed in this study has proven to be efficient in modeling pipelines subjected to relative soil movement and could be adapted for similar applications.

Acknowledgments

This research is supported by the Natural Sciences and Engineering Research Council of Canada (NSERC). Financial support provided by McGill Engineering Doctoral Award (MEDA) to the first author is appreciated.

References

- Ahmed, M. R., Tran, V. D. H., and Meguid, M. A. (2015). "On the role of geogrid reinforcement in reducing earth pressure on buried pipes: Experimental and numerical investigations." *Soils Found.*, 55(3), 588–599.
- Almahakeri, M., Moore, I. D., and Fam, A. (2016). "Numerical study of longitudinal bending in buried GFRP pipes subjected to lateral earth movements." *J. Pipeline Syst. Eng. Pract.*, 10.1061/(ASCE)PS.1949-1204.0000237, 04016012.
- ASCE. (1984). "Guidelines for the seismic design of oil and gas pipeline systems, committee on gas and liquid fuel lifelines." New York.
- Chan, P. D. S., and Wong, R. C. K. (2004). "Performance evaluation of a buried steel pipe in a moving slope: A case study." *Can. Geotech. J.*, 41(5), 894–907.
- Cui, L., and O'Sullivan, C. (2006). "Exploring the macro-and micro-scale response of an idealized granular material in the direct shear apparatus." *Geotechnique*, 56(7), 455–468.
- Cundall, P. A., and Strack, O. D. (1979). "A discrete numerical model for granular assemblies." *Geotechnique*, 29(1), 47–65.
- Daiyan, N., Kenny, S., Phillips, R., and Popescu, R. (2011). "Investigating pipeline-soil interaction under axial-lateral relative movements in the sand." *Can. Geotech. J.*, 48(11), 1683–1695.
- European Gas Pipeline Incident Data Group. (2005). "6th EGIG Report 1970–2004." *Rep. No. EGIG 05-R-0002*, Groningen, Netherlands.
- Guo, P. J., and Stolle, D. F. E. (2005). "Lateral pipe-soil interaction in sand with reference to scale effect." *J. Geotech. Geoenviron. Eng.*, 10.1061/(ASCE)1090-0241(2005)131:3(338), 338–349.
- Hoeg, K. (1968). "Stresses against underground structural cylinders." *J. Soil Mech. Found.*, 94(4), 833–858.
- Honegger, D. G., and Nyman, D. J. (2002). "Guidelines for the seismic design and assessment of natural gas and liquid hydrocarbon pipelines." Pipeline Research Council International, Arlington, VA.
- Hughes, T. J. R. (1995). "Multiscale phenomena: Green's functions, the Dirichlet-to-Neumann formulation, subgrid scale models, bubbles and the origins of stabilized methods." *Comput. Methods Appl. Mech. Eng.*, 127(1), 387–401.
- Karimian, H. (2006). "Response of buried steel pipelines subjected to longitudinal and transverse ground movement." Ph.D. thesis, Dept. of Civil Engineering, Univ. of British Columbia, Vancouver, BC, Canada.
- Karimian, H., Wijewickreme, D., and Honegger, D. (2006). "Buried pipelines subjected to transverse ground movement: Comparison between full-scale testing and numerical modeling." *Proc., 25th Int. Conf. on Offshore Mechanics and Arctic Engineering*, ASME, New York, 73–79.
- Kozicki, J., and Donzé, V. F. (2008). "A new open-source software developed for numerical simulations using discrete modeling methods." *Comput. Methods Appl. Mech. Eng.*, 197(49-50), 4429–4443.
- Labra, C., and Oñate, E. (2009). "High density sphere packing for discrete element method simulations." *Commun. Numer. Methods Eng.*, 25(7), 837–849.
- Ladd, R. S. (1978). "Preparing test specimens using undercompaction." *Geotech. Test. J.*, 1(1), 16–23.
- Liu, R., Guo, S., and Yan, S. (2015). "Study on the lateral soil resistance acting on the buried pipeline." *J. Coastal Res.*, 73, 391–398.
- Newmark, M., and Hall, W. J. (1975). "Pipeline design to resist large fault displacement." *Proc., U.S. National Conf. on Earthquake Engineering*, Earthquake Engineering Research Institute, Oakland, CA, 416–425.
- O'Rourke, M. J., and Nordberg, C. (1992). "Longitudinal permanent ground deformation effects on buried continuous pipelines." *Technical Rep. NCEER-92-0014*, National Center for Earthquake Engineering Research, Buffalo, NY.
- O'Sullivan, C. (2011). *Particulate discrete element modeling, a geomechanics perspective*, Spon Press, New York.
- PFC 2D version 3 [Computer software]. Itasca Consulting Group, Minneapolis.
- Plassiard, J.-P., Belheine, N., and Donzé, F.-V. (2009). "A spherical discrete element model: Calibration procedure and incremental response." *Granular Matter*, 11(5), 293–306.
- Potyondy, D. O., and Cundall, P. A. (2004). "A bonded-particle model for rock." *Int. J. Rock Mech. Min. Sci.*, 41(8), 1329–1364.
- Rahman, M. A., and Taniyama, H. (2015). "Analysis of a buried pipeline subjected to fault displacement: A DEM and FEM study." *Soil Dyn. Earthquake Eng.*, 71, 49–62.
- Šmilauer, V., et al. (2010). "The Yade project." (<http://yadedem.org/doc/>) (Oct. 28, 2013).
- Tran, V. D. H., Meguid, M. A., and Chouinard, L. E. (2013). "A finite-discrete element framework for the 3D modeling of geogrid-soil interaction under pullout loading conditions." *Geotext. Geomembr.*, 37(1), 1–9.
- Tran, V. D. H., Meguid, M. A., and Chouinard, L. E. (2014). "Discrete element and experimental investigations of the earth pressure distribution on cylindrical shafts." *Int. J. Geomech.*, 10.1061/(ASCE)GM.1943-5622.0000277, 80–91.
- Trautmann, C. H., and O'Rourke, T. D. (1983). "Behavior of pipe with dry sand under lateral and uplift loading." *Geotechnical Engineering Rep. 83-7*, Cornell Univ., Ithaca, NY.
- Wijewickreme, D., Karimian, H., and Honegger, D. (2009). "Response of buried steel pipelines subjected to relative axial soil movement." *Can. Geotech. J.*, 46(7), 735–752.
- Yan, W. M. (2008). "Effects of particle shape and microstructure on strength and dilatancy during a numerical direct shear test." *Proc., 12th Int. Association for Computer Methods and Advances in Geomechanics*, India, 1340–1345.
- Yimsiri, S., Soga, K., Yoshizaki, K., Dasari, G. R., and O'Rourke, T. D. (2004). "Lateral and upward soil-pipeline interactions in sand for deep embedment conditions." *J. Geotech. Geoenviron. Eng.*, 10.1061/(ASCE)1090-0241(2004)130:8(830), 830–842.
- Zhang, J., Liang, Z., and Han, C. (2016). "Mechanical behavior analysis of the buried steel pipeline crossing landslide area." *J. Pressure Vessel Technol.*, 138(5), 051702.
- Zienkiewicz, O. C., and Huang, G. C. (1990). "A note on localization phenomena and adaptive finite-element analysis in forming processes." *Commun. Appl. Numer. Methods*, 6(2), 71–76.